MODULAR CLIMBING ROBOT DESIGN WITH AUTOMATED VISION-BASED DEFECT CLASSIFICATION

Peter O. Oyekola[1]*, Shoeb Ahmed Syed[2]

[1] Department of Mechanical Engineering, Tennessee Tech University, Cookeville, USA
[2] Department of Mechanical Engineering, Papua New Guinea University of Technology, PNG
* pooyekola42@tntech.edu

In the examination of critical infrastructure for failure, common problems faced are restricted access to the inspection site, size and geometry constraints, cost, and extended inspection period. Facilities such as marine vessels, petrochemical pressure vessels, rail lines, and airplane fuselage, are regularly inspected. Mostly manual techniques with sensors like cameras and non-destructive testing kits are usually employed in detecting structural defects such as cracks and corrosion which constitute the central part of the cost and time spent. This paper, therefore, describes the design of a modular climbing robot for industrial inspection of structures. The main aim of improving and automating defect classification and identification is achieved by applying computer vision with an embedded wireless camera. YOLOv4 machine learning algorithm is implemented to identify and classify surface cracks and corrosion. The robot design combines a set of 6-DOF modular arm and tracked locomotion system. Embedded magnets are integrated into the design to aid navigation on vertical ferromagnetic structures and uneven surfaces. The final design shows that the robot can successfully navigate ferromagnetic structures, detect defects, and climb over moderately sized obstacles without loss of adhesion. This ensures performance in unfriendly and inaccessible environments, reducing costs and inspection time considerably.

Keywords: 6-DOF manipulator, computer vision, climbing robot, crack, corrosion, inspection robot

1 INTRODUCTION

For an exhaustive inspection of facility conditions, a thorough analysis of all structures must be done. In a bid to achieve this, access to some restricting points might be unsuccessful due to the possible presence of toxic chemicals, confined spaces, or high temperatures. There are several inspection techniques currently being utilized in the industry and the choice of techniques to apply depends on the nature of the inspection [1]. In carrying out inspections, workers might be placed in compromising health hazards such as heights, confined spaces, toxic environment, high temperatures, etc. This issue is further compounded by the use of crude equipment and tools such as ladders which could potentially increase the risk of slipping and falling from a height, scaffolds erection which is time-consuming as lots of time is spent on assembling and dismounting, and manual climbing, rigging which involves the use of rigging cables and supported platform, etc.

There has been an increasing demand for the requirements of robotic systems in an unstructured environment. This requires a careful redesign such that the robot must be capable of handling environment variations and operation assignments through an adaptable design. Robot autonomy in exploration, localization, surface mapping, path planning, and motion control are some of the outputs of recent advancements in robotic intelligence. These have been expanded further to the application of artificial intelligence in robot automation [2]. Computer vision with its vast engineering application is now being implemented in robotic systems for the automation of navigation, obstacle avoidance, defect detection, etc. using mounted cameras on robotic systems with direct onboard or remote processing [1]. Training a vision model to properly identify and classify defects involves gathering a large number of training datasets to increase its efficiency [3].

Inspection robot applications over the past decade are seen in technical inspection and maintenance such as failure or breakdown diagnosis [4], pipeline and turbine inspection [3], [5], [6] surface flaw detection of tanks and offshore platforms [7], power plants [8], Non-destructive testing [9] and in the aviation industry for inspection [10]. Furthermore, robots have also been applied in the inspection of civil structures [11], military and cleaning operations [12] Inspection of welds [13], marine environment for hull porosity and cracks [14], container inspection [15], aircraft structural inspection [16] [10].

1.1 Locomotion Mechanism

The method of locomotion of robots is of critical importance as it can dictate mobility principle, operating environment, operational speed as well as affect the efficiency of the overall system. Generally utilized locomotive systems are the tracked system, legged, wheeled, and sliding systems [17] [18]. For situations where terrains are uneven and rough, a legged robot is considered more suitable as they utilize discrete points on the terrain rather than requiring a large contact area for movement. Also, there is more flexibility and mobility in terms of degrees of freedom of the legged joints which can be extended while maintaining body position at a constant body level thereby controlling the robot's center of gravity which makes the robot less likely to tip over or fall [19] [20].

Wheel and track systems, on the other hand, are limited in application, significantly increase the weight and volume of the structure, but are faster and can support complex superimposed mechanisms. They are relatively more straightforward and cost less to build than the legged system. This mechanism is best suited for a relatively even terrain however, the tracked system could transverse uneven, rocky, and even swampy terrain to a degree [21]. Sliding robots employ an adhesion mechanism such as magnetic or suction cups and clutches for gripping the surface to allow for subsequent sliding of a movable section [22], [23].

1.2 Adhesion Mechanism

Vacuum adhesion (negative pressure), dry adhesion, and electrostatic adhesion mechanisms have been widely adopted in adhering to structures. However, the application of rare earth metals in magnetic adhesion has been practically explored given its energy-saving advantage. In principle, heavy actuators and robotic systems with large payloads can only be used vertically on ferromagnetic structures like storage tanks, containers, vessel hulls, etc. [24].

In suction systems, vacuum pressure is applied in sustaining adhesion to the structure. Vacuum is usually produced using suction engines, external hydraulic, plunger pump, centrifugal impeller, or passive suction cups [25]–[27] which create the negative pressure in the suction cup or chamber for wall-climbing. This can be applied to a variety of structures and materials (including non-ferromagnetic surfaces). Its main drawback however is the amount of vacuum required to achieve the desired adhesive force which also increases power requirement, a significant delay in achieving pressure which reduces operational speed in uneven structures with surface irregularity, and the presence of gaps between the surface and suction cups may prevent adhesion which causes detachment.

Dry adhesion (Van Der Waals force) is inspired by wall geckos' adhesion to surfaces without slipping or falling [28]. Van Der Waals forces are generated between the surface and the microfiber tape attached to the robot. For movement to occur, gradual loading increases the adhesion force of the robot, by peeling away from the surface, the adhesion force is reduced and moved to another point on the surface[18], [19]. Electrostatic adhesion however relied on an opposite induced charge between the structure and an adhesive pad near the surface. Although this can be applied on wood and glad surfaces, it is only suited for low-weight and short-distance applications [29].

The magnetic adhesion mechanism is more favored in industrial robots due to its reliability, efficiency, large adhesive force, and speed of operation although it requires the use of a heavy actuator as in the case of electromagnet application. This mechanism is only suited for navigation over ferromagnetic structures when the main goal is vertical navigation. This makes it unsuitable for use in most civil or structural applications like concrete or glass structures. Electromagnets or permanent magnets could be used to generate the adhesive force required in combination with wheels or tracks [30]. The adhesion force is determined by the magnetic properties of the type of magnets used, characteristics of the structure, and distance between the surface and the suction mechanism.

This study aims at developing a climbing robot for the industrial application while applying automated visual inspection in the identification and classification of defects. The robot is designed with the magnetic adhesion mechanism made of N52 grade neodymium magnets embedded in a track-driven chassis due to the requirement of high traction, speed, and obstacle maneuverability.

2 MATERIAL & METHOD

The robot design in this paper is expected to meet the mobility requirements of industrial application scenarios such as inspection of tall structures [31] [32] [33]. The general performance requirements were however limited to a lightweight and mobile design, multi-directional motion ability, sufficient traction, and adhesion on surfaces irrespective of positional orientation as well as safe navigation over moderate obstacles such as weld joints, rivets joints, etc. hence the conceptual model of the chassis is designed to support the load from a robot arm assembly, battery, electronic components as well as the camera mount both on horizontal and inclines surfaces. The main chassis is made of stainless steel, the robot arm is made of aluminum alloy, and the tracks are zinc due to weight consideration.

The robot power supply was regulated by a 12V Battery Management System (BMS) to prevent overcurrent or overvoltage. The main driving motor was powered by a 12V battery while a 5V DC supply powered the servo motor (6 for the robot arm and 2 for the pan and tilt mount) as well as the onboard computer as shown in figure 1.
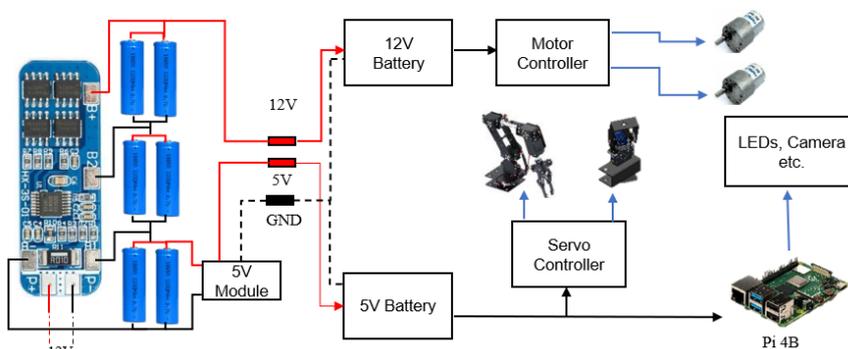

Fig 1: BMS connection, Electrical block diagram

Journal of Applied Engineering Science

Vol. 21, No. 1, 2023

www.engineeringscience.rs

iipp
publishing

Peter O. Oyekola et al. - Modular climbing robot design with automated vision-based defect classification

In training the detection model, 1500 training data sets of industrial cracks and corrosion were obtained from site visits and open-sourced images available online. Subsequently, all datasets were annotated before inputting into the YOLOv4 architecture which adopted a Single Shot Detection (SSD) model in defect identification. This open-source variety of the COCO-weighted model conveniently balances speed and performance during real-time inspection with assistance from a GPU-enabled computer. The model was finally tested by superimposing the model predictions of defects on a real-time streaming video output which can be viewed remotely.

3 ANALYSIS

3.1 Robot arm analysis

The arm kinematics were based on the Denavit-Hartenberg (DH) notation, and the parameter of the robot arm are shown in table 1. The simulation and experimental results of the manipulator were obtained by an evaluation of the kinematics following predefined paths before setting different scenarios and patterns of obstacles with distinct dimensions and parameters which were randomly placed. All of the test samples were strategically placed within the robot arm workspace, which represented the nominal setting for the manipulator while considering its dimensions. This ensured smooth and continuous operation of the arm to avoid unnecessary redundancies which are usually exploited when the arm reaches its limits. However, in practical arm control, the operator can determine the robot's position by implementing the forward kinematics as seen in the formulation below.

Table 1. link parameters for the robot arm

Joint (i)	Joint Angle (θ_i)	Distance (d_i mm)	Length (α_i mm)	Twist Angle (α_i deg)
1	θ_1	70	0	90
2	θ_2	0	105	0
3	θ_3	0	128	0
4	θ_4	0	70	0
5	θ_5	0	0	-90
6	θ_6	10	0	0

From figure 2, di (offset) represents the distance between the axis of rotation xi to xi+1 in the direction of zi. Similarly, the length of the links ai represents the distance measured from zi to zi+1 when estimated along zi. The angle of twist is represented as αi which indicates the angle between zi to zi+1 when estimated along xi. on the other hand, the angle measured between xi to xi+1 along zi is represented as θi. all these quantities are parameters of both the joint and link i.
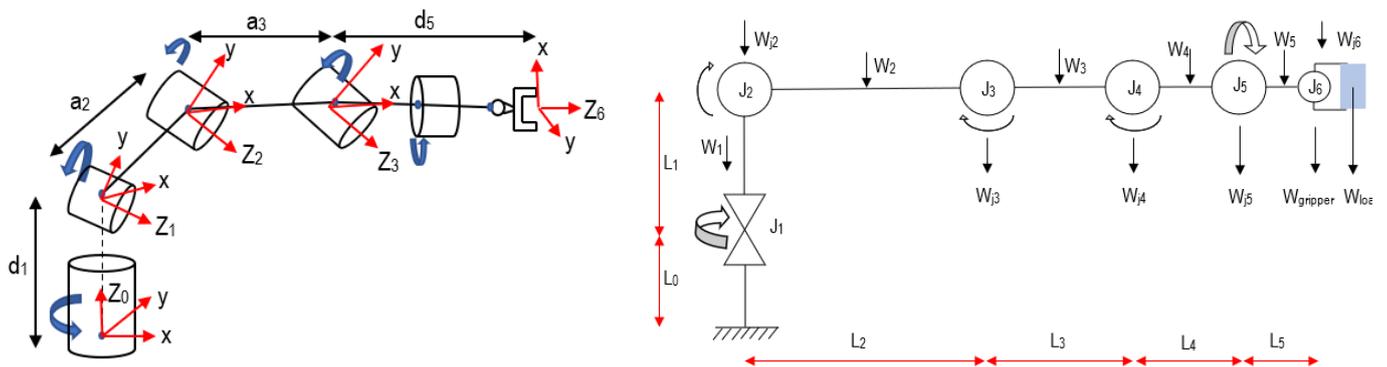

Fig 2: (a) Manipulator kinematic model (b) Freebody diagram at maximum torque pose

In Denavit-Hartenberg's convention, each homogenous transformational matrix T_i forms the product of the four transformations as in the equation below:

$$T_i = Rot(z, \theta_i).Trans(x, d_i).Trans(x, a_i).Rot(x, \alpha_i) = \begin{bmatrix} cos\theta_i & -sin\theta_i cos\alpha_i & sin\theta_i sin\alpha_i & a_i cos\theta_i \\ sin\theta_i & cos\theta_i cos\alpha_i & -cos\theta_i sin\alpha_i & a_i sin\theta_i \\ 0 & sin\alpha_i & cos\alpha_i & d_i \\ 0 & 0 & 0 & 1 \end{bmatrix} \quad (1)$$

Where Rot = angle rotation, and trans relates to the translation by a distance of the parameters below,

Journal of Applied Engineering Science

Vol. 21, No. 1, 2023

www.engineeringscience.rs

iipp

publishing

Peter O. Oyekola et al. - Modular climbing robot design with automated vision-based defect classification

$$Rot(z,\theta_i) = \begin{bmatrix} cos\theta_i & -sin\theta_i & 0 & 0 \\ sin\theta_i & cos\theta_i & 0 & 0 \\ 0 & 0 & 1 & 0 \\ 0 & 0 & 0 & 1 \end{bmatrix}, Trans(x,d_i) = \begin{bmatrix} 1 & 0 & 0 & 0 \\ 0 & 1 & 0 & 0 \\ 0 & 0 & 1 & d_i \\ 0 & 0 & 0 & 1 \end{bmatrix}$$

$$Trans(x,a_i) = \begin{bmatrix} 1 & 0 & 0 & a_i \\ 0 & 1 & 0 & 0 \\ 0 & 0 & 1 & 0 \\ 0 & 0 & 0 & 1 \end{bmatrix}, Rot(x,\alpha_i) = \begin{bmatrix} 1 & 0 & 0 & 0 \\ 0 & cos\alpha_i & -sin\alpha_i & 0 \\ 0 & sin\alpha_i & cos\alpha_i & 0 \\ 0 & 0 & 0 & 1 \end{bmatrix} \quad (2)$$

This transformation represents the resultant transformation of any two joints. From the manipulator parameters of the individual transformation matrices $T_1^0, T_2^1, \ldots T_5^0$, the matrix transformation for T_5^0 can be utilised in establishing the position and the orientation of the mechanical claw relative to the robot's base. Where,

$$T_5^0 = T_1^0 \times T_2^1 \times \ldots \times T_5^4 = \begin{bmatrix} c_{1,5}c_{2+3+4} + s_{1,5} & -c_1 s_{2+3+4} s_5 + s_1 c_5 & c_1 c_{2+3+4} & c_1(d_5 c_{2+3+4} + a_3 c_{2+3} + a_2 c_2) \\ s_1 c_5 c_{2+3+4} - c_1 s_5 & -s_{1,4} s_{2+3+4} + c_{1,5} & s_1 c_{2+3+4} & s_1(d_5 c_{2+3+4} + a_4 c_{2+3} + a_2 c_2) \\ -c_{2+3+4}c_5 & c_{2+3+4}s_5 & -s_{2+3+4} & d_1 - a_2 c_2 - a_2 s_{2+3} - d_5 s_{2+3+4} \\ 0 & 0 & 0 & 1 \end{bmatrix} \quad (3)$$

Where Ci represents cosine and Si is the sine of the angle. From the resulting matrix, the elements in the last column indicated the location (l_x, l_y and l_z) of the end effector (Gripper) while other elements indicate its vector alignment which is effectively represented by:

$$T_5^0 = \begin{bmatrix} n_x & o_x & a_x & l_x \\ n_y & o_y & a_y & l_y \\ n_z & o_z & a_z & l_z \\ 0 & 0 & 0 & 1 \end{bmatrix} \quad (4)$$

This formulation can therefore be implemented in the robot arm control through a slider widget on the remote computer. This gives the operator a higher degree of control as necessitated by the uncertainty of application.

3.2 Servo Motors Torque Determination

The resistive torque acting on the joints are dynamic as it varies based on the respective position and poses assumed by the robot at any point in time. The effective force at the shoulder joint is far greater while the arm at a fully horizontal position which is the worst possible position that can be assumed by the arm to exert the highest torque [34]. Figure 2b shows the free body representation of the maximum torque pose Where Li = lengths, Ji = joints, Wi = Weight of component, and Wji = Weight of respective joint servo. Subsequently, the resistive torque Tgi exerted on the joints as a result of gravity is shown below given that the base rotation does not interfere with the motion of other links in the vertical plane,

$$T_{g1} = W_{j2}.Lsin180 = 0 \text{ Kg. cm} \quad (5)$$

$$T_{g2} = W_2\frac{L_2}{2} + W_3\left(L_2 + \frac{L_3}{2}\right)\frac{L_2}{2} + W_{j3}(L_2) + W_{j4}(L_{2+3}) + W_4\left(L_{2+3} + \frac{L_4}{2}\right) + W_{j5}(L_{2+3+4}) + W_5\left(L_{2+3+4} + \frac{L_5}{2}\right) + W_T(L_{2+3+4+5}) = 6.263 \text{ Kg. cm} \quad (6)$$

$$T_{g3} = W_3\frac{L_3}{2} + W_{j4}(L_3) + W_{j4}(L_{2+3}) + W_4\left(L_3 + \frac{L_4}{2}\right) + W_{j5}(L_{3+4}) + W_5\left(L_{3+4} + \frac{L_5}{2}\right) + W_T(L_{3+4+5}) = 4.489 \text{ Kg. cm} \quad (7)$$

$$T_{g4} = W_4\frac{L_4}{2} + W_{j5}(L_4) + W_5\left(L_4 + \frac{L_5}{2}\right) + W_T(L_{4+5}) = 4.103 \text{ Kg. cm} \quad (8)$$

$$T_{g5} = W_5\left(\frac{L_5}{2}\right) + \left(W_g + W_l + W_{j6}\right)(L_5) = 2.082 \text{ Kg. cm} \quad (9)$$

$$T_{g6} = W_T\left(\frac{1}{2}L_g\right) = 0.463 \text{ Kg. cm} \quad (10)$$

Where $W_T = W_g + W_l + W_{j6}$ \quad (11)

3.3 Servo Selection

The selection of suitable servo motor was based on the estimation of the moment of inertia which is the resistance of the joints to rotation change [35]. the parallel axis theorem applied considered the arm pivots around the base servo which is not the center of mass. Therefore, the moment of inertia of the new axis can be mathematically expressed as;

$$I = I_{cm} + md^2 \quad (12)$$

where the estimation of the mass moment of inertia for each link is estimated and given as;

$$T_{i1} = [(I_{zz,s1} + m_{s1}d_{11}{}^2) + (I_{zz,s2} + m_{s2}d_{12}{}^2) + (I_{zz,l2} + m_{l2}d_{13}{}^2) + (I_{zz,s3} + m_{s3}d_{14}{}^2) + (I_{zz,l3} + m_{l3}d_{15}{}^2) + (I_{zz,s4} + m_{s4}d_{16}{}^2) + (I_{zz,l4} + m_{l4}d_{17}{}^2) + (I_{zz,s5} + m_{s5}d_{18}{}^2) + (I_{zz,s6} + m_{s6}d_{19}{}^2) + (I_{zz,g} + m_g d_{110}{}^2)] \propto \qquad (13)$$

$$T_{i2} = [(I_{xx,l2} + m_{l2}d_{21}{}^2) + (I_{xx,s3} + m_{s3}d_{22}{}^2) + (I_{xx,l3} + m_{l3}d_{23}{}^2) + (I_{xx,s4} + m_{s4}d_{24}{}^2) + (I_{xx,l4} + m_{l4}d_{25}{}^2) + (I_{xx,s5} + m_{s5}d_{26}{}^2) + (I_{xx,s6} + m_{s6}d_{27}{}^2) + (I_{xx,g} + m_g d_{28}{}^2)] \propto \qquad (14)$$

$$T_{i3} = [(I_{xx,l3} + m_{l3}d_{31}{}^2) + (I_{xx,s4} + m_{s4}d_{32}{}^2) + (I_{xx,l4} + m_{l4}d_{33}{}^2) + (I_{xx,s5} + m_{s5}d_{34}{}^2) + (I_{xx,s6} + m_{s6}d_{35}{}^2) + (I_{xx,g} + m_g d_{36}{}^2)] \propto \qquad (15)$$

$$T_{i4} = [(I_{xx,l4} + m_{l4}d_{41}{}^2) + (I_{xx,s5} + m_{s5}d_{42}{}^2) + (I_{xx,s6} + m_{s6}d_{43}{}^2) + (I_{xx,g} + m_g d_{44}{}^2)] \propto \qquad (16)$$

$$T_{i5} = [(I_{yy,s6} + m_{s6}d_{51}{}^2) + (I_{yy,g} + m_g d_{52}{}^2)] \propto \qquad (17)$$

Where T_{ix} = inertia induced resistive torque at the joints, I_{base} = servo moment of inertia, I_{Lx} = link moment of inertia, M_{sx} = mass of servos, and m_{L1} = mass of links

Based on these estimations, the selected servo motor was a DT-3316 20MG High torque model across all the joints. This was controlled using pulse width modulation signals which determine the shaft position within a 180-degree range.

3.4 Robot Chassis

The final robot model had a total dimension of 320 mm X 250 mm X 160 mm excluding the mounted robot arm which falls within the range of commercially available inspection robots. The track's front and rear ends are inclines and have an angle of 45^0 and 30^0 respectively to enable navigation over obstacles such as weld seams and uneven surfaces (see figure 6).

Additionally, the total weight of the full assembly was 6.2 Kg. The values of size to weight factors offer the application of the designed model where requirements for autonomous control as well as the installation of additional payloads for inspections and testing are needed. The total model was further optimized by building a second model with a total weight of 2.2 Kg to maximize adhesion with lower power requirements.

To allow for ease of control, the chain tracks are mounted directly on a set of driving gears and bearings which are connected directly to the output shaft of the motor gearbox. This eliminated the need for additional transmissions given that the propulsion system and arm account for the highest power consumption.

4 MAGNETOSTATICS ANALYSIS

The adhesion module of the robot was simulated using EMWORKS (EMS 2017) to optimize the adhesion force created by the N52 grade magnet as well as to understand the variable factors which affect the magnet adaptation. This is critical given that the robot is expected to support its weight and safely navigate over obstacles without slip or loss of adhesion. The result of parameters such as air gap distance, the distance between magnets, angle of inclination as well as physical dimensions of the selected magnet is shown in figures 3 and 4. The result indicates that the optimal configuration for maximum adhesion force is with a 1 mm air gap and 12 mm distance between magnet and magnet dimension of 20mm yoke thickness and 25mm width.
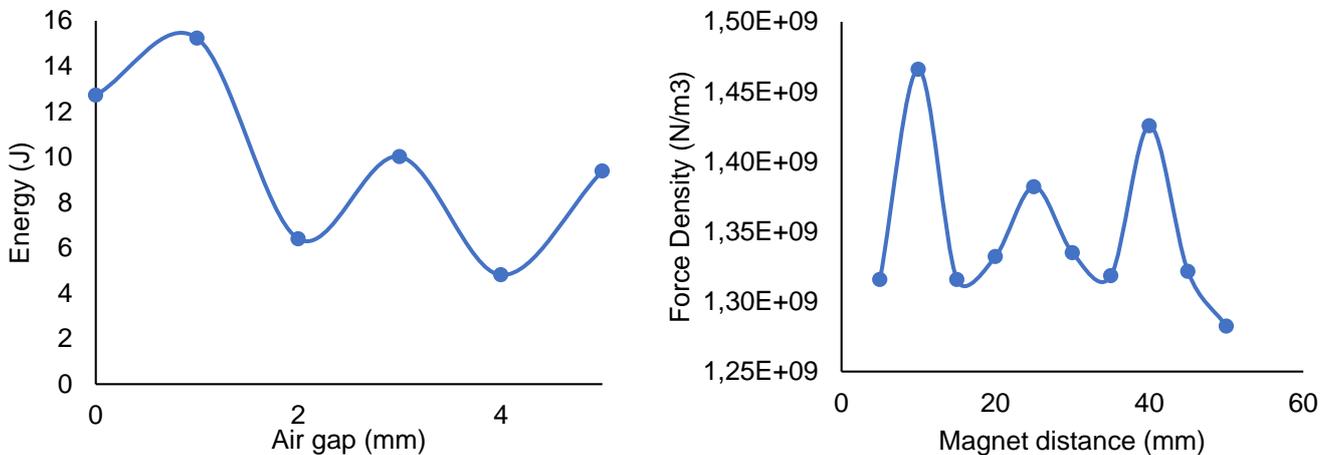

Fig 3: (a) varying air gap (b) varying magnet distance

Journal of Applied Engineering Science

Vol. 21, No. 1, 2023

www.engineeringscience.rs

iipp
publishing

Peter O. Oyekola et al. - Modular climbing robot design with automated vision-based defect classification
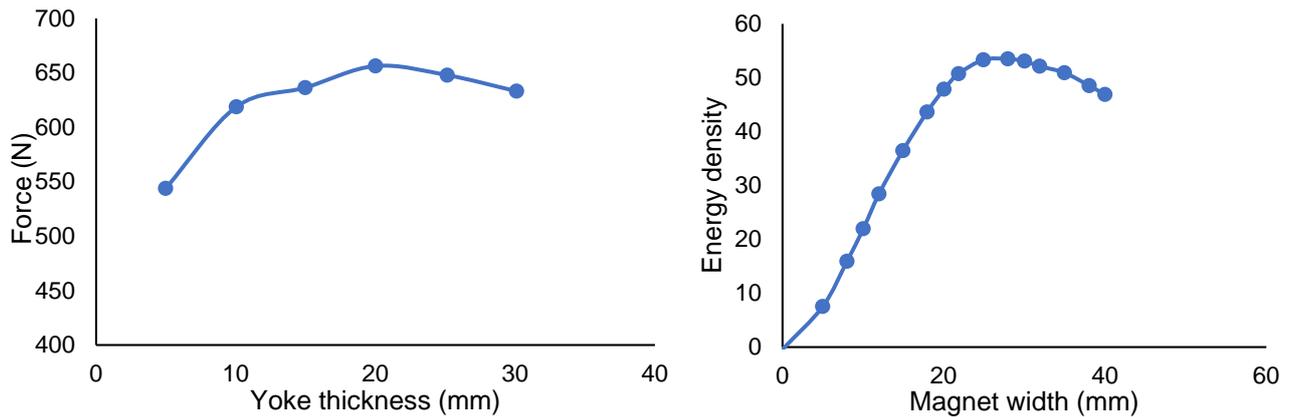
Fig 4: Effect of yoke thickness and magnet width on adhesion

5 DISCUSSION

Commercially available parts were sourced for the generic design of the robot which was equipped with both computational and long-range control capabilities. The tracking mechanism employed also allows for navigation over rough and unstructured terrains although this does not permit wall transition as seen in the work of Changmin et al [36]. This was subsequently tested, and the results are shown in figure 5. Due to the total weight of the first model, the overall total speed and climbing angle was significantly limited where practical tests showed that slip starts to occur at angles of 35 degrees and more. This is attributed to the low coefficient of friction between the zinc alloy track implemented and the test surface. From the optimized model which had significant weight reduction, the maximum robot horizontal speed was 2.97km/h with a maximum climbing angle of 150 degrees with a speed of 0.45km/h. the robots are also able to navigate small obstacles up to 60mm and 10 mm respectively without loss of adhesion. This result is comparable to the robot designed by Xianlei Chen et al [37] whose robot weighs a total of 9.5kg and was able to navigate vertical structures for tank volume calibration.

The geometry of the robot design was selected primarily based on a reduced distance between to inspection surface to the center of mass of the robot. Increased distance would invariably increase the probability of robot detachment from the adhered surface either under its weight or because of gravity on the robot. This is readily seen when comparing the two-robot design. Robot one has a much higher center of mass compared to robot two and hence robot two performed better with the ability to navigate even while hanging over a 180-degree rotated plane.
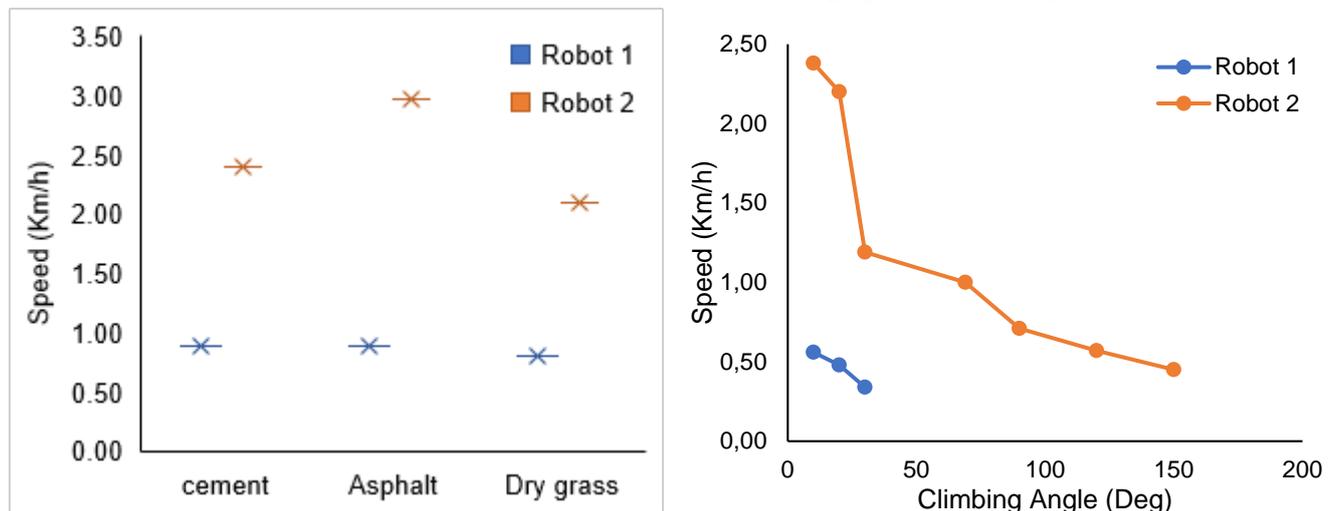

Fig 5: (a) Robot's horizontal speed across terrains (b) Climbing speed

5.1 Defect identification

In validating the defect identification system, the test was conducted using sample images not used during the model training process as well as a live field test to verify optimal functionality under varying light conditions and exposure levels. The final model had a training accuracy of 91% maximum after about 6000 iterations, after which there is no further increase in accuracy of detection. This indicated the model's ability to identify even small defects. Sources of errors in the detection model were primarily due to improper annotation of objects. A more precise annotation will prevent interference in the identification of defects during real-time trials.

Journal of Applied Engineering Science

Vol. 21, No. 1, 2023

www.engineeringscience.rs

iipp
publishing

Peter O. Oyekola et al. - Modular climbing robot design with automated vision-based defect classification
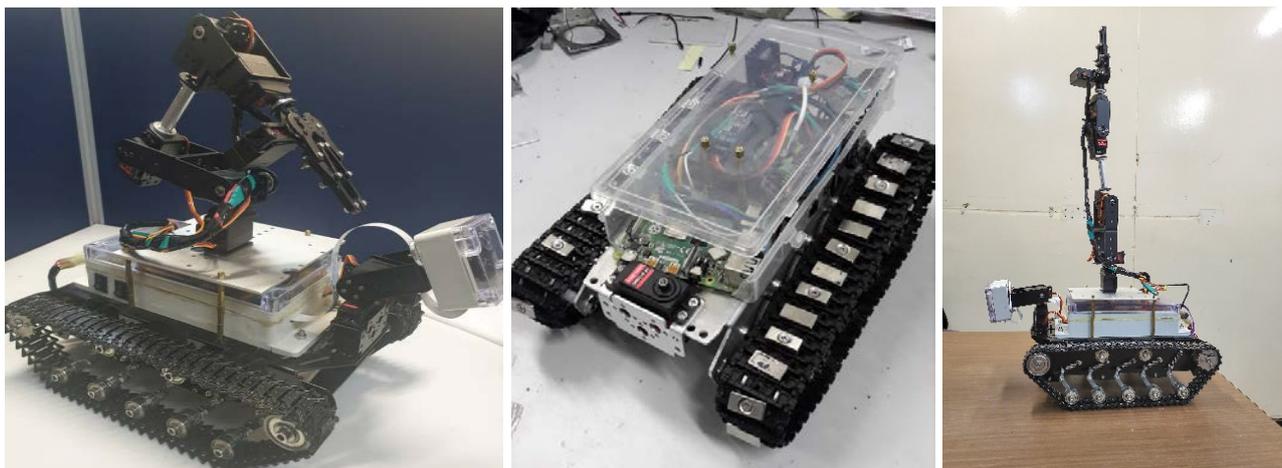
Fig 6: Mechanical robot models

Also, field testing showed that while cracks were perfectly detected at varying lighting conditions, corrosion, however, could not be detected using the installed night vision mode while operating in dark regions such as in enclosed spaces. This is due to the color-dependent training adopted i.e., most data used for corrosion contained brownish red discoloration. But in the night vision mode, the camera image becomes greyscale hence the difficulty in identifying the trend except when LED lights are used instead of the infrared lights installed on the camera.

Fig 7: Sample automatic defect detections

6 CONCLUSION & FUTURE WORK

This paper discussed the design of a modular climbing robot that integrated a 6-DOF manipulator and applied computer vision in the automated detection of industrial defects. In achieving an optimal design, a set of model parameters concerning the design variables was parameterized and used to derive a nominal design of the robot using commercially available parts. The manipulator was based on Denavit-Hartenberg's convention for optimization which was simulated on MATLAB to optimize the arm kinematics.

The adhesion and locomotion system was achieved using Neodymium N52 grade magnets installed on the outer surface of the robot tracks and optimized using EMWORKS to optimize the necessary adhesion force required to keep the robot firmly attached to the surface even while navigating over moderately sized obstacles commonly found in the industry. The defect identification model was processed directly from the onboard Raspberry Pi computer which also controlled the navigation and data acquisition. The model had a 91% accuracy limit based on the available amount of training dataset employed in the study. The confidence threshold was left at 25% for reduced false detections

Although the designed model is a basic foundational model, it can be improved by design optimization for less weight, proper material selection, provision for plane transition or higher obstacles climbing ability, as well as the implementation of a variable speed controller which eases the robot's control in high-speed operations.

7 REFERENCE

[1] P. Oyekola, A. Mohamed, and J. Pumwa, "Robotic model for unmanned crack and corrosion inspection," International Journal of Innovative Technology and Exploring Engineering, vol. 9, no. 1, pp. 862–867, Nov. 2019, doi: 10.35940/ijitee.A4367.119119.

[2] A. S. Rajawat, R. Rawat, K. Barhanpurkar, R. N. Shaw, and A. Ghosh, "Robotic process automation with increasing productivity and improving product quality using artificial intelligence and machine learning," in Artificial Intelligence for Future Generation Robotics, Elsevier, 2021, pp. 1–13.

[3]   P. O. Oyekola, S. Kolawole, S. A. Syed, and O. Apis, "Application of Computer Vision in Pipeline Inspection Robot," 2021.

[4]   A. Skoczylas, P. Stefaniak, S. Anufriiev, and B. Jachnik, "Belt conveyors rollers diagnostics based on acoustic signal collected using autonomous legged inspection robot," Applied Sciences, vol. 11, no. 5, p. 2299, 2021.

[5]   M. Fisher et al., "An overview of verification and validation challenges for inspection robots," Robotics, vol. 10, no. 2, p. 67, 2021.

[6]   M. Z. Ab Rashid, M. F. M. Yakub, S. A. Z. bin Shaikh Salim, N. Mamat, S. M. S. M. Putra, and S. A. Roslan, "Modeling of the in-pipe inspection robot: A comprehensive review," Ocean Engineering, vol. 203, p. 107206, 2020.

[7]   Saiigdeok Park, Hee Don Jeong, and Zhong Soo Lim, "Design of a mobile robot system for automatic integrity evaluation of large size reservoirs and pipelines in industrial fields," 2004. doi: 10.1109/iros.2003.1249265.

[8]   J. Wang, J. Huang, and R. Cheng, "Automatic reading system for analog instruments based on computer vision and inspection robot for power plant," in 2018 10th International Conference on Modelling, Identification and Control (ICMIC), 2018, pp. 1–6.

[9]   H. Ahmed, H. M. La, and N. Gucunski, "Review of non-destructive civil infrastructure evaluation for bridges: State-of-the-art robotic platforms, sensors and algorithms," Sensors, vol. 20, no. 14, p. 3954, 2020.

[10] A. Perelli, L. De Marchi, A. Marzani, and S. Freear, "Compressive Sensing for Damage Detection in Composite Aircraft Wings," Structural Health Monitoring 2013, Vols 1 and 2, 2013.

[11] C. Yuan, B. Xiong, X. Li, X. Sang, and Q. Kong, "A novel intelligent inspection robot with deep stereo vision for three-dimensional concrete damage detection and quantification," Structural Health Monitoring, vol. 21, no. 3, pp. 788–802, 2022.

[12] N. Elkmann, T. Felsch, M. Sack, J. Saenz, and J. Hortig, "Innovative service robot systems for facade cleaning of difficult-to-access areas," IEEE International Conference on Intelligent Robots and Systems, 2002, doi: 10.1109/IRDS.2002.1041481.

[13] J. Li, S. Jin, C. Wang, J. Xue, and X. Wang, "Weld line recognition and path planning with spherical tank inspection robots," Journal of Field Robotics, vol. 39, no. 2, pp. 131–152, 2022.

[14] R. Enjikalayil Abdulkader, P. Veerajagadheswar, N. Htet Lin, S. Kumaran, S. R. Vishaal, and R. E. Mohan, "Sparrow: A magnetic climbing robot for autonomous thickness measurement in ship hull maintenance," Journal of Marine Science and Engineering, vol. 8, no. 6, p. 469, 2020.

[15] W. Shen, J. Gu, and Y. Shen, "Permanent Magnetic System Design for the Wall-Climbing Robot," Applied Bionics and Biomechanics, 2015, doi: 10.1155/2006/143256.

[16] G. Niu, J. Wang, and K. Xu, "Model analysis for a continuum aircraft fuel tank inspection robot based on the Rzeppa universal joint," Advances in Mechanical Engineering, vol. 10, no. 5, p. 1687814018778229, 2018.

[17] W. Guo, M. Zhong, M. T. Li, and Y. Li, "Design of a six legged wall-climbing robot," 2008. doi: 10.1109/ARSO.2008.4653597.

[18] Y. Liu, S. Sun, X. Wu, and T. Mei, "A leg-wheel wall-climbing robot utilizing bio-inspired spine feet," 2013. doi: 10.1109/ROBIO.2013.6739732.

[19] K. A. Daltorio et al., "Mini-whegsTM climbs steep surfaces using insect-inspired attachment mechanisms," International Journal of Robotics Research, 2009, doi: 10.1177/0278364908095334.

[20] P. Boscariol, M. A. Henrey, Y. Li, and C. Menon, "Optimal Gait for Bioinspired Climbing Robots Using Dry Adhesion: A Quasi-Static Investigation," Journal of Bionic Engineering, 2013, doi: 10.1016/S1672-6529(13)60193-6.

[21] C. Balaguer, A. Gimenez, and A. Jordon, "Climbing robots' mobility for inspection and maintenance of 3D complex environments," Autonomous Robots, 2005, doi: 10.1007/s10514-005-0723-0.

[22] S. Wu, L. Wu, and T. Liu, "Design of a sliding wall climbing robot with a novel negative adsorption device," 2011. doi: 10.1109/URAI.2011.6145940.

[23] R. Lal Tummala et al., "Climbing the walls [robots]," IEEE Robotics & Automation Magazine, 2003, doi: 10.1109/mra.2002.1160067.

[24] R. D. Dethe and S. B. Jaju, "Developments in wall climbing robots: a review," International journal of engineering research and general science, vol. 2, no. 3, pp. 33–42, 2014.

[25] H. Albitar, A. Ananiev, and I. Kalaykov, "New concept of in-water surface cleaning robot," 2013. doi: 10.1109/ICMA.2013.6618150.

[26] Y. Yoshida and S. Ma, "A wall-climbing robot without any active suction mechanisms," 2011. doi: 10.1109/ROBIO.2011.6181587.

[27] J. Gu, C. Wang, and X. Wu, "Self-adjusted adsorption strategy for an aircraft skin inspection robot," Journal of Mechanical Science and Technology, vol. 32, no. 6, pp. 2867–2875, 2018.

[28] M. Carlo and S. Metin, "A Biomimetic Climbing Robot Based on the Gecko," Journal of Bionic Engineering, 2006, doi: 10.1016/S1672-6529(06)60015-2.

[29] K. H. Koh, R. M. Kuppan Chetty, and S. G. Ponnambalam, "Modeling and simulation of electrostatic adhesion for wall climbing robot," 2011. doi: 10.1109/ROBIO.2011.6181590.

[30] J. Sánchez, F. Vázquez, and E. Paz, "Machine vision guidance system for a modular climbing robot used in shipbuilding," 2006. doi: 10.1007/3-540-26415-9-107.

[31] "Robotics - Standards | Occupational Safety and Health Administration." https://www.osha.gov/robotics/standards (accessed Aug. 19, 2022).

[32] "Standards, Guidelines & Industry Best Practices for Industrial & Collaborative Robots | RoboticsTomorrow." https://roboticstomorrow.com/article/2021/08/standards-guidelines-industry-best-practices-for-industrial-collaborative-robots/17289 (accessed Aug. 19, 2022).

[33] M. Oitzman, "Mobile Robot Standards," Mobile Robot Guide, May 18, 2021. https://mobilerobotguide.com/2021/05/18/mobile-robot-standards/ (accessed Aug. 19, 2022).

[34] A. M. Mohamed, Z. A. Zyada, and E. A. El-Shenawy, "Design, modeling and control of a wall climbing robot crossingover obstacles," 2014 IEEE/SICE International Symposium on System Integration, SII 2014, pp. 46–51, 2014, doi: 10.1109/SII.2014.7028009.

[35] C. D. Bellicoso, L. R. Buonocore, V. Lippiello, and B. Siciliano, "Design, modeling and control of a 5-DoF light-weight robot arm for aerial manipulation," 2015. doi: 10.1109/MED.2015.7158852.

[36] C. Park, J. Bae, S. Ryu, J. Lee, and T. Seo, "R-track: separable modular climbing robot design for wall-to-wall transition," IEEE Robotics and Automation Letters, vol. 6, no. 2, pp. 1036–1042, 2020.

[37] X. Chen, Y. Wu, H. Hao, H. Shi, and H. Huang, "Tracked wall-climbing robot for calibration of large vertical metal tanks," Applied Sciences, vol. 9, no. 13, p. 2671, 2019.